Inorganic Chemistry
Article

Inorg. Chem. **2009**, *48*, 10697–10702 **10697**
DOI: 10.1021/ic9014652

Ag/AgBr/$WO_3 \cdot H_2O$: Visible-Light Photocatalyst for Bacteria Destruction

Peng Wang,[†] Baibiao Huang,*[,†] Xiaoyan Qin,[†] Xiaoyang Zhang,[†] Ying Dai,[‡] and Myung-Hwan Whangbo[§]

[†]*State Key Lab of Crystal Materials, Shandong University, Jinan 250100, China,* [‡]*School of Physics, Shandong University, Jinan 250100, China, and* [§]*Department of Chemistry, North Carolina State University, Raleigh, North Carolina 27695-8204*

Received July 23, 2009

A new composite photocatalyst Ag/AgBr/$WO_3 \cdot H_2O$ was synthesized by reacting $Ag_8W_4O_{16}$ with HBr and then reducing some Ag^+ ions in the surface region of AgBr particles to Ag nanoparticles via the light-induced chemical reduction. Ag nanoparticles are formed from AgBr by the light-induced chemical reduction reaction. The Ag/AgBr particles are on the surface of $WO_3 \cdot H_2O$ and have irregular shapes with sizes varying between 63 and 442 nm. $WO_3 \cdot H_2O$ appears as flakes about 31 nm thick and 157−474 nm wide. The as-grown Ag/AgBr/$WO_3 \cdot H_2O$ sample shows strong absorption in the visible region because of the plasmon resonance of Ag nanoparticles in Ag/AgBr/$WO_3 \cdot H_2O$. The ability of this compound to destroy *E. coli* and oxidize methylic orange under visible light was compared with those of other reference photocatalysts. Ag/AgBr/$WO_3 \cdot H_2O$ is a highly efficient photocatalyst under visible light. The Ag/AgBr/$WO_3 \cdot H_2O$ samples recovered from repeated photooxidation experiments are almost identical to the as-prepared samples, proving the stability of Ag/AgBr/$WO_3 \cdot H_2O$ sample.

1. Introduction

Since the discovery of photocatalytic destruction of microbial cells with TiO_2 by Matsunaga et al.[1] in 1985, semiconductor-based materials have been extensively investigated as photocatalysts for bacteria destruction.[2−6] Due to its high chemical stability, good photoactivity, relatively low cost, and nontoxicity, TiO_2 has appeared as a leading candidate. However, its photocatalytic activity requires ultraviolet (UV) light ($\lambda < 400$ nm), which provides sufficient energy for the electron excitation across its band gap (i.e., 3.2 eV for anatase TiO_2). Only about 4% of the solar spectrum can be utilized by pure TiO_2, and the ultraviolet light is harmful. Thus, it is of great interest to develop photocatalysts that can yield high reactivity under visible light so that a greater portion of the solar spectrum may be used to provide photocatalytic activity.[7−11] To extend the absorption band-edge of TiO_2 from UV to visible light region, a number of different approaches[12−16] have been developed, including doping[17−21] and combining TiO_2 with another semiconductor.[22−24] Hu et al.[25] demonstrated that AgBr on P-25 TiO_2 support is the main photoactive species

*To whom correspondence should be addressed. E-mail: bbhuang@sdu.edu.cn.

(1) Matsunaga, T.; Tomoda, R.; Nakajima, T.; Wake, H. *FEMS Microbiol. Lett*. **1985**, *29*, 211–214.
(2) Hu, X. X.; Hu, C.; Qu, J. H. *Appl. Catal. B: Environ*. **2006**, *69*, 17–23.
(3) Yu, H. T.; Quan, X.; Zhang, Y. B.; Ma, N.; Chen, S.; Zhao, H. M. *Langmuir* **2008**, *24*, 7599–7604.
(4) Schneider, O. D.; Loher, S.; Brunner, T. J.; Schmidlin, P.; Stark, W. J. *J. Mater. Chem*. **2008**, *18*, 2679–2684.
(5) Li, Q.; Xie, R. C.; Li, Y. W.; Mintz, E. A.; Shang, J. K. *Environ. Sci. Technol*. **2007**, *41*, 5050–5056.
(6) Li, H.; Ni, Y. H.; Cai, Y. F.; Zhang, L.; Zhou, J. Z.; Hong, J. M.; Wei, X. W. *J. Mater. Chem*. **2009**, *19*, 594–597.
(7) Beier, C. W.; Cuevas, M. A.; Brutchey, R. L. *Small* **2008**, *12*, 2102–2106.
(8) Gao, L.; Wang, Y.; Wang, J. Q.; Huang, L.; Shi, L. Y.; Fan, X. X.; Zou, Z. G.; Yu, T.; Zhu, M.; Li, Z. S. *Inorg. Chem*. **2006**, *45*, 6844–6850.
(9) Soni, S. S.; Henderson, M. J.; Bardeau, J. F.; Gibaud, A. *Adv. Mater*. **2008**, *20*, 1493–1498.
(10) Brezesinski, T.; Rohlfing, D. F.; Sallard, S.; Antonietti, M.; Smarsly, B. M. *Small* **2006**, *2*, 1203–1211.
(11) Lin, J.; Lin, J.; Zhu, Y. F. *Inorg. Chem*. **2007**, *46*, 8372–8378.
(12) Yurdakal, S.; Palmisano, G.; Loddo, V.; Augugliaro, V.; Palmisano, L. *J. Am. Chem. Soc*. **2008**, *130*, 1568–1569.
(13) Kim, T. W.; Hur, S. G.; Hwang, S. J.; Park, H.; Choi, W.; Choy, J. H. *Adv. Funct. Mater*. **2007**, *17*, 307–314.
(14) Iskandar, F.; Nandiyanto, A. B. D.; Yun, K. M.; Hogan, C. J.; Okuyama, K., Jr.; Biswas, P. *Adv. Mater*. **2007**, *19*, 1408–1412.
(15) Macak, J. M.; Zlamal, M.; Krysa, J.; Schmuki, P. *Small* **2007**, *3*, 300–304.
(16) Yu, J. C.; Li, G. S.; Wang, X. C.; Hu, X. L.; Leung, C. W.; Zhang, Z. D. *Chem. Commun*. **2006**, 2717–2719.
(17) Joung, S. K.; Amemiya, T.; Murabayashi, M.; Itoh, K. *Chem.—Eur. J*. **2006**, *12*, 5526–5534.
(18) Li, H. X.; Bian, Z. F.; Zhu, J.; Huo, Y. N.; Li, H.; Lu, Y. F. *J. Am. Chem. Soc*. **2007**, *129*, 4538–4539.
(19) Premkumar, J. *Chem. Mater*. **2005**, *17*, 944–946.
(20) Zhang, L. W.; Fu, H. B.; Zhu, Y. F. *Adv. Funct. Mater*. **2008**, *18*, 2180–2189.
(21) Sano, T.; Negishi, N.; Koike, K.; Takeuchi, K.; Matsuzawa, S. *J. Mater. Chem*. **2004**, *14*, 380–384.
(22) Kale, B. B.; Baeg, J. O.; Lee, S. M.; Chang, H.; Moon, S. J.; Lee, C. W. *Adv. Funct. Mater*. **2006**, *16*, 1349–1354.
(23) Liu, Z.; Sun, D. D.; Guo, P.; Leckie, J. O. *Nano Lett*. **2007**, *7*, 1081–1085.
(24) Kemell, M.; Pore, V.; Ritala, M.; Leskela, M.; Linden, M. *J. Am. Chem. Soc*. **2005**, *127*, 14178–14179.
(25) Hu, C.; Lan, Y.; Qu, J.; Hu, X.; Wang, A. *J. Phys. Chem. B* **2006**, *110*, 4066–4072.

© 2009 American Chemical Society
Published on Web 10/19/2009

for bacteria destruction under visible light. Their evidence indicates that AgBr is the visible-light active component of the catalyst, and that the Ag^0 species on the surface of the catalyst probably enhances the electron−hole separation and the interfacial charge transfer. Elahifard et al.[26] have reported that $Ag/AgBr/TiO_2$-covered apatite has a high ability for adsorbing bacteria in the dark and also has a significantly high photocatalytic activity under visible light. Despite extensive efforts, improving the photocatalytic activity of TiO_2 has met only a limited success. Therefore, it is desirable to develop a new type of photocatalyst with high photocatalytic activity.[27,28]

In recent years, a variety of metal complex oxides have also been found to exhibit photocatalytic activity.[29] It was demonstrated that the plasmon photocatalyst Ag@AgCl, i.e., AgCl powder particles with Ag nanoparticles adsorbed on their surface, is efficient and stable under visible light because the Ag nanoparticles strongly absorb visible light, prevent photogenerated electrons from combining with Ag^+ ions, and allow the formation of Cl^0 atoms by combining Cl^- ions with photogenerated holes.[30] The composite semiconductor $H_2WO_4 \cdot H_2O$/AgCl, i.e., AgCl particles adsorbed on the surface of $H_2WO_4 \cdot H_2O$ crystallites, was also found to be an efficient and stable photocatalyst under visible light.[31] $H_2WO_4 \cdot H_2O$ is a small band gap (SBG) semiconductor compared with AgCl, and the conduction band (CB) bottom and the valence band (VB) top of the SBG semiconductor $H_2WO_4 \cdot H_2O$ lie below the CB bottom and VB top of AgCl, respectively. Thus, in the composite semiconductor $H_2WO_4 \cdot H_2O$/AgCl, the photogenerated electrons are prevented from recombining with Ag+ ions, hence allowing the formation of Cl^0 atoms by combining Cl^- ions with photogenerated holes. Furthermore, it was observed that the plasmon photocatalyst Ag@AgBr is more efficient than is Ag@AgCl although Br0 has a lower oxidizing power than does Cl^0, because Br^- combines with a photogenerated hole faster than does Cl^-.[32] In general, photogenerated electrons in those photocatalysts are expected to be trapped by O_2 molecules in the solution to form superoxide ions (O_2^-) and other reactive oxygen species.[33]

The above discussion leads one to speculate if a composite semiconductor consisting of Ag, AgBr, and tungsten oxides might be a very efficient photocatalyst under visible light. Our synthetic efforts to prepare such a photocatalyst led to a new composite semiconductor $Ag/AgBr/WO_3 \cdot H_2O$. The CB bottom and VB top of AgBr are located at −3.7 and −5.95 eV, respectively.[34] Using the method described in ref 31, we found that the CB bottom and VB top of $WO_3 \cdot H_2O$ are located at −4.404 and −6.574 eV, respectively. Thus, in this composite semiconductor $Ag/AgBr/WO_3 \cdot H_2O$, the visible light can excite AgBr, $WO_3 \cdot H_2O$, and the Ag nanoparticles. As illustrated in Figure 1, it is expected that the photogenerated electrons transfer to Ag nanoparticles and are separated from the holes in the valence bands of AgBr and $WO_3 \cdot H_2O$. Then the separated holes would oxidize the organic compounds. Compared with the plasmon photocatalyst Ag@AgBr, the oxidizing ability of $Ag/AgBr/WO_3 \cdot H_2O$ would be higher, because the VB of $WO_3 \cdot H_2O$ is lower than that of AgBr. In the following, we show that the photocatalyst $Ag/AgBr/WO_3 \cdot H_2O$ has the advantages of a plasmon photocatalyst and a composite photocatalyst, is highly efficient in degradation of organic pollutants and *Escherichia coli* (*E. coli*), and is photostable under repeated use.

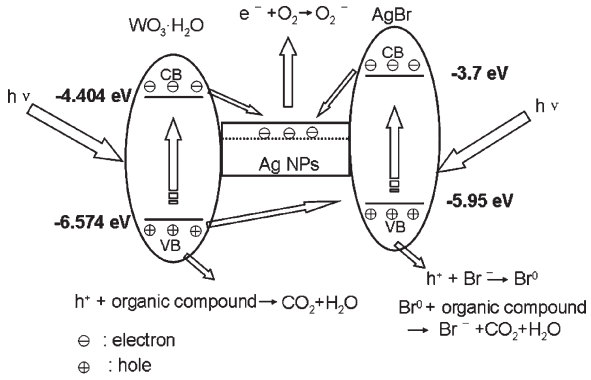

Figure 1. Schematic diagram illustrating the photogeneration of electrons/holes as well as their migration and reactions in the new composite semiconductor $Ag/AgBr/WO_3 \cdot H_2O$. The light-absorption generates electrons, e^-, at the bottom of the CB and holes, h^+, at the top of the CB in AgBr and $WO_3 \cdot H_2O$. The electrons e^- of both AgBr and $WO_3 \cdot H_2O$ migrate into the Ag nanoparticles. The holes h^+ of $WO_3 \cdot H_2O$ can migrate into AgBr. The expected reactions of the holes of $WO_3 \cdot H_2O$ and AgBr and the electrons of Ag nanoparticles are also shown.

2. Experiment Section

2.1. Synthesis of the Starting Material $Ag_8W_4O_{16}$. $Ag_8W_4O_{16}$ was prepared by a microwave-assisted hydrothermal reaction. An aqueous solution of $AgNO_3$ and that of Na_2WO_4 were prepared in advance. Ten mL of 0.2 M $AgNO_3$ solution was mixed with 10 mL of 0.1 M Na_2WO_4 solution, without adjusting the pH value of the mixed solution. The resulting solution was stirred for about 0.5 h, transferred into a special Teflon autoclave, and then heated at 180 °C for 1 h under microwave radiation, which led to the precipitation of $Ag_8W_4O_{16}$. The $Ag_8W_4O_{16}$ precipitate was collected and washed with deionized water until the pH value of the washing solution was about 7, and dried in air.

2.2. Synthesis of the Photocatalyst $Ag/AgBr/WO_3 \cdot H_2O$. $AgBr/WO_3 \cdot H_2O$ was synthesized by the ion exchange reaction between $Ag_8W_4O_{16}$ and concentrated HBr while sonicating the solution until the completion of the ion exchange process, as described in our previous work.[32] $AgBr/WO_3 \cdot H_2O$ was synthesized by the hydrobromic acid treated process between $Ag_8W_4O_{16}$ and concentrated HBr while sonicating the solution until the completion of the hydrobromic acid treated process. The precipitate was collected, washed with deionized water, and dried at 70 °C for 8 h. Then the $AgBr/WO_3 \cdot H_2O$

(26) Elahifard, M. R.; Rahimnejad, S.; Haghighi, S.; Gholami, M. R. *J. Am. Chem. Soc.* **2007**, *129*, 9552–9553.
(27) Reddy, V. R.; Currao, A.; Calzaferri, G. *J. Mater. Chem.* **2007**, *17*, 3603–3609.
(28) Kong, L. D.; Chen, H. H.; Hua, W. M.; Zhang, S. C.; Chen, J. M. *Chem. Commun.* **2008**, 4977–4979.
(29) Wang, D.; Kako, T.; Ye, J. *J. Am. Chem. Soc.* **2008**, *130*, 2724–2725.
(30) Wang, P.; Huang, B. B.; Qin, X. Y.; Zhang, X. Y.; Dai, Y.; Wei, J. Y.; Whangbo, M.-H. *Angew. Chem.* **2008**, *120*, 8049–8051.
(31) Wang, P.; Huang, B. B.; Zhang, X. Y.; Qin, X. Y.; Dai, Y.; Jin, H.; Wei, J. Y.; Whangbo, M.-H. *Chem.—Eur. J.* **2008**, *14*, 10543–10546.
(32) Wang, P.; Huang, B. B.; Zhang, X. Y.; Qin, X. Y.; Hao, J.; Dai, Y.; Wang, Z. Y.; Wei, J. Y.; Zhan, J.; Wang, S. Y.; Wang, J. P.; Whangbo, M.-H. *Chem.—Eur. J.* **2009**, *15*, 1821–1824.
(33) Hoffmann, M. R.; Martin, S. T.; Choi, W.; Bahnemann, D. W. *Chem. Rev.* **1995**, *95*, 69–96.
(34) Seki, K.; Yanagi, H.; Kobayashi, Y.; Ohta, T.; Tani, T. *Phy. Rev. B* **1994**, *49*, 2760–2767.

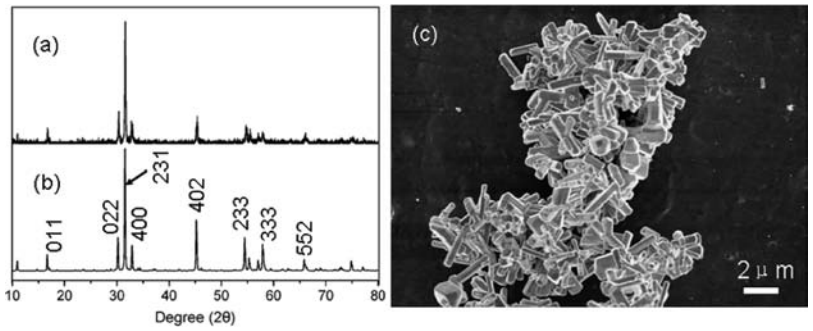

Figure 2. (a) XRD pattern of the as-prepared $Ag_8W_4O_{16}$ sample. (b) XRD pattern of the standard $Ag_8W_4O_{16}$ (JCPDS file 70-1719) . (c) Typical SEM image of $Ag_8W_4O_{16}$.

powder was put into a solution of MO dye, which was then irradiated with a 300 W Xe arc lamp (PLS-SXE300, Beijing Trusttech Co. Ltd.) equipped with an ultraviolet cutoff filter to provide visible light with $\lambda \geq 400$ nm. Then the resulting precipitate, which consisted of silver nanoparticles, was washed and dried in air.

The crystal structure of the sample was examined by X-ray diffraction (XRD) (Bruker AXS D8), its morphology was examined by scanning electron microscopy (SEM) (Hitachi S-4800 microscopy), and its diffuse reflectance was examined by UV/vis spectroscopy (UV-2550, Shimadzu).

2.3. Synthesis of the Reference Photocatalysts $WO_3 \cdot H_2O$ and N-TiO_2. A reference photocatalyst, $WO_3 \cdot H_2O$, was prepared using the method reported in the literature.[35] Another reference photocatalyst, N-doped TiO_2, was prepared by nitridation of commercially available TiO_2 powder (with surface area 50 m^2/g) at 773 K for 10 h under NH_3 flow (with the flow rate of 350 mL/min).[36]

2.4. Evaluation of Photocatalytic Activities. The photocatalytic activities of $WO_3 \cdot H_2O$, N-TiO_2 Ag/AgBr, and Ag/AgBr/$WO_3 \cdot H_2O$ for the destruction of *E. coli* were measured by using 10^7 colony-forming-units/mL (cfu/mL) bacterial-cell concentration. The photocatalytic reaction was started by irradiating the bacterial cell solution containing the photocatalyst under visible light ($\lambda \geq 400$ nm). A 300W Xe arc lamp (focused through a shutter window) with UV cutoff filter (providing visible light $\lambda \geq 400$ nm) was used as a light source. The reaction mixture was cooled by an ice/water mixture to prevent the influence of heat. During the reaction, the bacterial suspension was sampled at 10, 20, and 30 min. An aliquot of the reaction mixture was immediately diluted with sterile deionized water and spread uniformly onto a nutrient agar plate. After 24 h incubation at 37 °C, the number of viable cells was then determined by the plate count method. Photocatalytic degradation of MO dye was carried out with 0.2 g of the powdered photocatalyst suspended in 100 mL of MO dye solution prepared by dissolving 20 mg of MO powder in 1.0 L of distilled water in a pyrex-glass cell at room temperature under air. The degradation of MO dye was monitored by UV/vis spectroscopy (UV-7502PC, Xinmao, Shanghai).

(35) Shiba, F.; Yokoyama, M.; Mita, Y.; Yamakawa, T.; Okawa, Y. *Mater. Lett.* **2007**, *61*, 1778–1780.
(36) Maeda, K.; Shimodaira, Y.; Lee, B.; Teramura, K.; Lu, D.; Kobayashi, H.; Domen, K. *J. Phys. Chem. C* **2007**, *111*, 18264–18270.

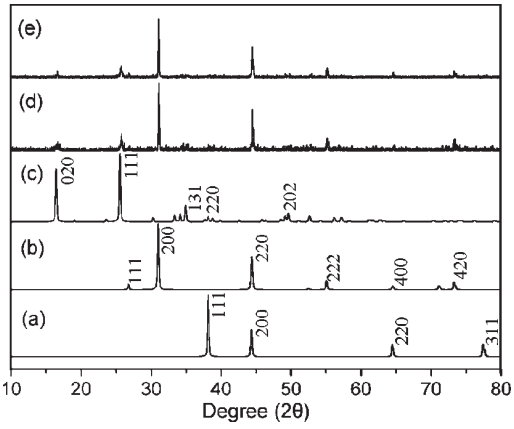

Figure 3. XRD patterns of (a) Ag, (b) AgBr, (c) $WO_3 \cdot H_2O$, (d) the as-prepared Ag/AgBr/$WO_3 \cdot H_2O$ and (e) the Ag/AgBr/$WO_3 \cdot H_2O$ used for six consecutive photooxidation experiments with the solution of MO dye under visible-light irradiation.

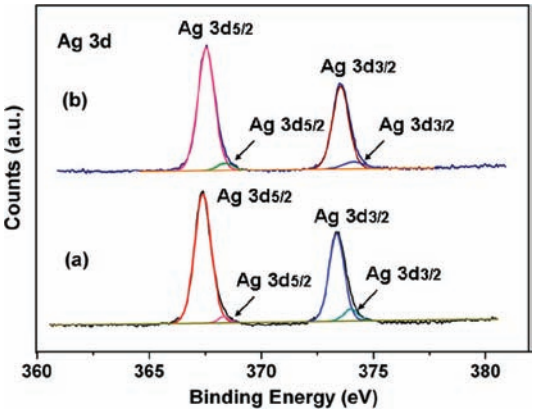

Figure 4. Ag 3d XPS spectras of (a) the as-prepared Ag/AgBr/$WO_3 \cdot H_2O$ and (b) the Ag/AgBr/$WO_3 \cdot H_2O$ used for six consecutive photooxidation experiments with the solution of MO dye under visible-light irradiation.

3. Results and Discussion

3.1. Crystal Structure and Morphology of the Starting Material $Ag_8W_4O_{16}$. The size and morphology of the composite photocatalyst Ag/AgBr/ $WO_3 \cdot H_2O$ depends on those of the starting material $Ag_8W_4O_{16}$. XRD analysis was carried out to investigate the crystal structure of the as-obtained $Ag_8W_4O_{16}$. The typical XRD pattern of the $Ag_8W_4O_{16}$ is given in Figure 2a. All the diffraction peaks could be indexed as the orthorhombic phase of $Ag_8W_4O_{16}$, and the lattice constants are a = 10.89 Å,

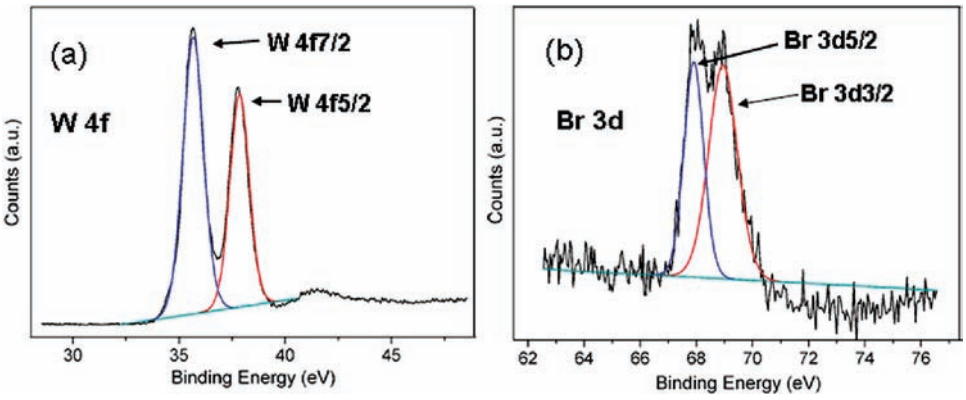

Figure 5. XPS spectra of (a) W 4f of the as prepared Ag/AgBr/$WO_3 \cdot H_2O$ and (b) the Br 3d of the Ag/AgBr/$WO_3 \cdot H_2O$.

$b = 12.03$ Å, and $c = 5.92$ Å in agreement with the standard data from JCPDS file 70-1719. The morphology and size of the starting material were investigated by SEM. Figure 2c shows the image of $Ag_8W_4O_{16}$, which appears as prism-like submicrometer particles of about 0.56−2.72 μm length, which can be normally explained by the outside embodiment of the unit-cell replication and amplification of the orthorhombic phase.

3.2. Characterization of the Photocatalyst Ag/AgBr/$WO_3 \cdot H_2O$. 3.2.1. XRD and XPS Analysis of Ag/AgBr/$WO_3 \cdot H_2O$. The XRD pattern of the Ag/AgBr/$WO_3 \cdot H_2O$ sample is shown in Figure 3, which shows the coexistence of AgBr (JCPDS file 6-438) and $WO_3 \cdot H_2O$ (JCPDS file 18-1418). The phase of AgBr is cubic, and the lattice constants are $a = 5.77$ Å in agreement with the standard date from the JCPDS. The phase of $WO_3 \cdot H_2O$ is orthorhombic with space group Pmnb and the lattice constants are $a = 5.24$ Å, $b = 10.78$ Å, and $c = 5.14$ Å in agreement with the standard data from the JCPDS. From the XRD result, the peaks in Figure 3a belonging to Ag (JCPDS file 65-2871) superpose on the peaks belonging to AgBr (Figure 3b; JCPDS file 6-438) and $WO_3 \cdot H_2O$ (Figure 1c; JCPDS file 18-1418), so it is difficult to draw any conclusions concerning the existence of Ag from the XRD measurements.

Thus the Ag/AgBr/$WO_3 \cdot H_2O$ sample was examined by X-ray photoelectron spectroscopy (XPS), and the results are shown in Figures 4 and 5. The binding energies of the XPS spectra were calibrated by C1s (284.8 eV). In Figure 4a, the Ag 3d spectra of Ag/AgBr/$WO_3 \cdot H_2O$ consist of two individual peaks at ~373 and ~367 eV, which can be attributed to Ag $3d_{3/2}$ and Ag $3d_{5/2}$ binding energies, respectively. The Ag $3d_{3/2}$ peak is further divided into two different peaks at 373.36 and 373.99 eV, and the Ag $3d_{5/2}$ peak is divided into two different peaks at 367.4 and 368.32 eV. According to Shah et al.,[37] the peaks at 373.99 and 368.32 eV are attributed to metal Ag^0 and the peaks at 367.4 and 373.36 eV are attributed to Ag^+ of AgBr, and those at 373.99 and 368.32 eV to metal Ag^0 hence confirming the existence of Ag^0. From the XPS peak areas, the surface Ag^0 and Ag^+ contents are calculated to be 0.61 and 8.18 mol %, respectively.

The W 4f spectra of Ag/AgBr/$WO_3 \cdot H_2O$ (Figure 5a) consists of two individual peaks W $4f_{5/2}$ and W $4f_{7/2}$, with binding energies ~37.83 and ~35.68 eV, respectively. The calculated surface W^{6+} contents of the sample is 29.53 mol %. The spectra of Br 3d in Figure 5b show that the binding energies of Br $3d_{3/2}$ and Br $3d_{5/2}$ are ~68.75 and ~67.75 eV, and the calculated surface Br^- content is 7.89 mol %. Thus, the observed ratio 8.18:29.53 of the surface Ag^+ and W^{6+} is considerably smaller than the ratio 2:1 expected from the formula of the starting material $Ag_8W_4O_{16}$. The most probable cause for the discrepancy is that, during the reaction between $Ag_8W_4O_{16}$ and concentrated HBr, some AgBr is formed and dissolved away in the superfluous HBr solution.

The O1s spectra are not shown because the content of O from the XPS result is not accurate. The O 1s spectra contain the contribution from the adsorbed O_2 during the sample preparation process for the XPS measurement.

3.2.2. Electron Microscopy Analysis and UV/vis Diffuse Reflectance Spectra of Ag/AgBr/ $WO_3 \cdot H_2O$. The SEM images of Figure 6 show the morphology of the

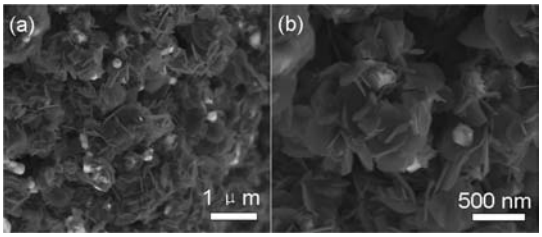

Figure 6. SEM images of Ag/AgBr/$WO_3 \cdot H_2O$.

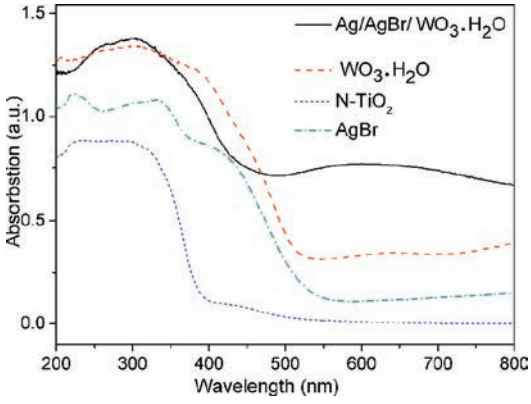

Figure 7. UV/vis diffuse reflectance spectra of Ag/AgBr/$WO_3 \cdot H_2O$, $WO_3 \cdot H_2O$, N-doped TiO_2, and AgBr.

(37) Shah, Md. S. A. S.; Nag, M.; Kalagara, T.; Singh, S.; Manorama, S. V. *Chem. Mater.* **2008**, *20*, 2455–2460.

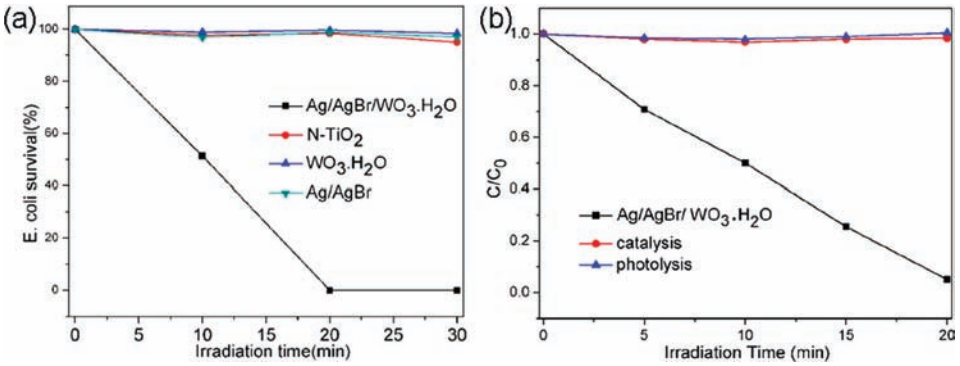

Figure 8. (a) Temporal course of the *E. coli* inactivation (1×10^7 cfu/mL, 10 mL) in aqueous dispersion containing 0.1 g/L catalyst ($Ag/AgBr/WO_3 \cdot H_2O$, $WO_3 \cdot H_2O$, N-doped TiO_2, and Ag/AgBr) under visible-light irradiation. (b) Photodecomposition of MO dye in solution (20 mg/L) over $Ag/AgBr/WO_3 \cdot H_2O$ under visible-light irradiation ($\lambda \geq 400$ nm), catalysis with $Ag/AgBr/WO_3 \cdot H_2O$ in the dark, and photolysis under full arc light irradiation without $Ag/AgBr/WO_3 \cdot H_2O$. C is the concentration of MO dye at time t, and C_0 is that in the MO solution immediately before it is kept in the dark.

as-prepared $Ag/AgBr/WO_3 \cdot H_2O$ sample. The Ag/AgBr particles, which appear as bright spots, are formed on the surface of $WO_3 \cdot H_2O$ and have irregular shapes with their sizes varying between 63 and 442 nm. $WO_3 \cdot H_2O$ appears as flakes about 31 nm thick and 157−474 nm wide. It is difficult to confirm the position and the size of the Ag nanoparticles. Higher resolution images can not be achieved because AgBr is decomposed by the high energy electron beam.

The UV/vis diffuse reflectance spectra of $Ag/AgBr/WO_3 \cdot H_2O$, $WO_3 \cdot H_2O$, AgBr, and N-doped TiO_2 are presented in Figure 7. AgBr, N-doped TiO_2, and $WO_3 \cdot H_2O$ have strong absorption in the UV region, but do not strongly absorb in the visible region. In contrast, the as-grown $Ag/AgBr/WO_3 \cdot H_2O$ samples have much stronger absorption in the visible region than do AgBr, N-doped TiO_2, and $WO_3 \cdot H_2O$. This can be ascribed to the plasmon resonance of Ag nanoparticles in $Ag/AgBr/WO_3 \cdot H_2O$.

3.2.3. Photocatalytic Activities for *E. coli* Destruction and MO Degradation. Figure 8a shows the photocatalytic destruction of *E. coli* over $WO_3 \cdot H_2O$, N-TiO_2, Ag/AgBr, and $Ag/AgBr/WO_3 \cdot H_2O$ photocatalysts. Unlike $WO_3 \cdot H_2O$ N-TiO_2 and Ag/AgBr, $Ag/AgBr/WO_3 \cdot H_2O$ exhibits a high photcatalytic activity under visible light. Nearly half the amount of *E. coli* is photocatalytically destroyed after only 10 min of irradiation, and almost all of the *E. coli* are destroyed after 20 min of irradiation, while more than 95% and of the *E. coli* are still alive with $WO_3 \cdot H_2O$, N-TiO_2, and Ag/AgBr. The results can also be seen from the representative photographs of the *E. coli* colonies (Figure 9). The results show that the Ag nanoparticles formed from AgBr do not play an important role in the antibacterial process because both Ag/AgBr and Ag/AgCl can not destroy *E. coli* under visible light. This indicates that the holes in the VB of $WO_3 \cdot H_2O$ oxidize the cell wall of the *E. coli* finally destroying it.

The degradation experiments in the dark with $Ag/AgBr/WO_3 \cdot H_2O$ and under full arc light irradiation without $Ag/AgBr/WO_3 \cdot H_2O$ were also carried out. In these experiments, the *E. coli* concentration remained unchanged demonstrating that $Ag/AgBr/WO_3 \cdot H_2O$ is a visible light photocatalyst for bacteria destruction.

The photooxidation capability of $Ag/AgBr/WO_3 \cdot H_2O$ was also evaluated by measuring the decomposition of methylic orange (MO) dye in the MO solution (with

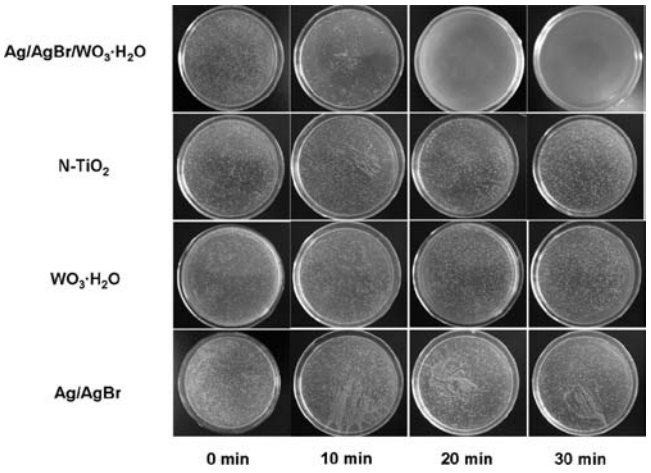

Figure 9. Photographs of the *E. coli* colonies in the antibacterial experiment.

concentration of 20 mg/L) over the $Ag/AgBr/WO_3 \cdot H_2O$ sample under visible-light irradiation ($\lambda \geq 400$ nm). The decomposition over the $Ag/AgBr/WO_3 \cdot H_2O$ catalyst is completed in 20 min of visible-light irradiation (Figure 8b). The decomposition experiments in the dark with $Ag/AgBr/WO_3 \cdot H_2O$ (catalysis) and under full arc light irradiation without $Ag/AgBr/WO_3 \cdot H_2O$ (photolysis) were also carried out. In these experiments, the MO concentration remained unchanged as a function of time thereby demonstrating that $Ag/AgBr/WO_3 \cdot H_2O$ is a photocatalyst active under visible light.

3.3. Stability of $Ag/AgBr/WO_3 \cdot H_2O$. The repeated MO-bleaching experiment on $Ag/AgBr/WO_3 \cdot H_2O$ was also examined. After the fifth consecutive run, the bleaching rate was slightly decreased because the amount of $Ag/AgBr/WO_3 \cdot H_2O$ in the reactor was reduced due to the sampling of the slurry at every measurement of the MO concentration. To check the stability of $Ag/AgBr/WO_3 \cdot H_2O$, the sample used for six consecutive bleaching experiments was examined by XRD and XPS. The XRD pattern (Figure 3e) was almost identical to that of the as-prepared samples. The XPS spectrum (Figure 4b) is also almost identical to those of the as-prepared sample. The calculated contents of the surface Ag of the corresponding samples are 0.67 mol %. The change in the Ag content is in the error range of the apparatus. Thus, the

$Ag/AgBr/WO_3 \cdot H_2O$ sample is stable under our experimental conditions.

4. Conclusions

The composite semiconductor $Ag/AgBr/WO_3 \cdot H_2O$ with Ag/AgBr particles on the surface of $WO_3 \cdot H_2O$, synthesized in the present study, has strong absorption in the visible region due to the plasmon resonance of the Ag nanoparticles on AgBr, exhibits a superior photocatalytic activity for the destruction of *E. coli* under visible light irradiation, and is quite stable under repeated use. This composite semiconductor has the advantages of a plasmon photocatalyst and a composite photocatalyst. Our study strongly suggests that useful photocatalysts active in visible light can be found by integrating metal nanoparticles with plasmon resonance into composite semiconductors with appropriate band gaps and band gap edges.

Acknowledgment. This work was financially supported by the National Basic Research Program of China (973 Program, Grant 2007CB613302), and the National Natural Science Foundation of China under Grants 50721002, 10774091, and 20973102. M.-H.W. thanks the support by the Office of Basic Energy Sciences, Division of Materials Sciences, U.S. Department of Energy, under Grant DE-FG02-86ER45259.